Successive magnetic field-induced transitions and colossal magnetoelectric effect in Ni_3TeO_6

Jae Wook Kim[1,2],* S. Artyukhin[3],* E. D. Mun[1], M. Jaime[1], N. Harrison[1],
A. Hansen[1], J. J. Yang[2], Y. S. Oh[2], D. Vanderbilt[3], V. S. Zapf[1], and S.-W. Cheong[2]
[1]*Los Alamos National Laboratory (LANL), Los Alamos, NM 87545, USA*
[2]*Rutgers Center for Emergent Materials and Department of Physics and Astronomy, Rutgers University, Piscataway, NJ 08854, USA and*
[3]*IAMDN and Department of Physics and Astronomy, Rutgers University, Piscataway, NJ 08854, USA*
(Dated: December 9, 2014)

Ni_3TeO_6 was recently shown to have magnetic field-induced spin-flop transition that produces a record large non-hysteretic magnetoelectric coupling ($\alpha = 1300$ ps/m). Here we measure magnetic, electric and structural properties of Ni_3TeO_6 single crystals over the majority of its $H-T$ phase diagram for magnetic fields up to 92 T and temperatures down to 1.5 K and discover an additional field-induced phase transition at 52 T, accompanied by the polarization change of 3 mC/m^2, among the largest magnetically induced polarization changes observed. With the help of density-functional calculations we construct a microscopic model that describes the data, model the spin structures across the whole field range, and clarify the physics behind the second transition. We answer the question of why the magnetically induced polarization at the high field transition is so much larger than at the first transition and identify the dominant magnetic exchange path, which drives the polarization change via the exchange striction mechanism.

Magnetoelectric (ME) multiferroics have been extensively studied recently to understand the mechanisms responsible for cross-coupling between magnetism and ferroelectricity, which is at the heart of their promise for application in multifunctional devices [1–6]. In this class of materials, at least three mechanisms are known to induce ferroelectric polarization (P) upon magnetic order: (1) the spin current or inverse Dzyaloshinskii-Moriya (DM) interaction in a spin-cycloidal structure which is mediated by anti-symmetric exchange [7–9], (2) the symmetric exchange-striction mechanism between parallel or anti-parallel alignment of spins [10], and (3) the hybridization between metal d and ligand p orbitals that is modulated by spin direction [11]. A majority of magnetoelectric couplings that have been studied to date involve mechanisms (1) and (3). However, the symmetric exchange mechanism (2) can, in principle, also lead to large ME effects. An archetypical example of this mechanism is the spin-chain multiferroic compound $Ca_3(Co,Mn)O_6$, where Co and Mn spins form an $\uparrow\uparrow\downarrow\downarrow$ structure along the c-axis at zero field, breaking spatial inversion symmetry along the chain with strong easy-axis anisotropy [10]. However, the ME coupling α ($\equiv dP/dH$) in $Ca_3(Co,Mn)O_6$ is relatively weak, with $\alpha \approx 100$ ps/m.

Ni_3TeO_6 (NTO) belongs to a family of corundum-related compounds M_3TeO_6 (M = Mn, Co, Ni, and Cu) that has recently attracted interest in light of various magnetic structure depending on M-site ions and ME coupling, and consequently, various mechanisms of ME coupling [12–19]. Mn_3TeO_6 and Co_3TeO_6 show complex magnetic phase diagrams with commensurate or incommensurate magnetic ordering [15, 16] while Cu_3TeO_6 shows commensurate order with multiple AFM domains [20]. Magnetically-induced electric polarization, P, observed in Co_3TeO_6, is most likely induced by inverse DM effect [14]. Multiple field-induced transitions are also found in Co_3TeO_6 where a low-field canted antiferromagnetic (AFM) structure is transformed to spin-flop state with large hysteresis [21].

NTO crystallizes in a $R3$ space group with three Ni ions ($3d^8$, S = 1) and a non-magnetic Te ion arranged along the c-axis in a unit cell (Fig. 1) to form a linear chain with broken spatial inversion symmetry. This material is a pyroelectric, but in addition to its unswitchable polarization component due to the polar structure, it also shows a large magnetically induced polarization. In zero magnetic field (H), NTO has a collinear $\uparrow\uparrow\uparrow\downarrow\downarrow\downarrow$ AFM order [13] with spins along the c-axis and a Neél temperature (T_N) of 52 K. This ordering is similar to that in $Ca_3(Co,Mn)O_6$ [10, 22], where an electric polarization is induced by exchange-striction mechanism.

Recently, a second-order spin-flop (SF) transition at a critical field $H_{c1} \sim 9$ T was observed in NTO, which is accompanied by a large ME effect [19]. The ME coefficient $\alpha \equiv dP/dH$ is as high as 1300 ps/m at H_{c1}, without any magnetic hysteresis. This is another example of strong ME coupling due to the symmetric exchange striction. Here, symmetric exchange striction at the SF transition distorts the polar crystal structure to modify the electric polarization.

In this Letter, we present a high-magnetic-field study (up to 92 T) of NTO and report the discovery of a new magnetic-field-induced phase transition, which is accompanied by a colossal ME effect. In the $H \parallel c$ configuration, a magnetic transition occurs at H_{c2} = 52 T with a ~ 3 mC/m^2 drop in P at 4 K. For $H \parallel ab$ plane, a sharp cusp in the $\Delta P(H)$ curve was observed at ~ 70 T. We corroborate our experimental results with microscopic modeling, using model parameters extracted from extensive density-functional theory (DFT) calculations, thereby predicting the magnetic structure at all magnetic fields. Multiple exchange interactions are found to contribute to the field-dependence of electric polarization via an exchange striction mechanism. Compared to its isostructural compounds Mn_3TeO_6 and Co_3TeO_6, which show multiferroic behavior by antisymmetric exchange interaction [14–16], NTO exhibits an exchange-striction driven polarization response that is almost two orders of magnitude larger, thereby demonstrating a unique behavior in this class of materials.

Single crystals of NTO were grown by chemical vapor

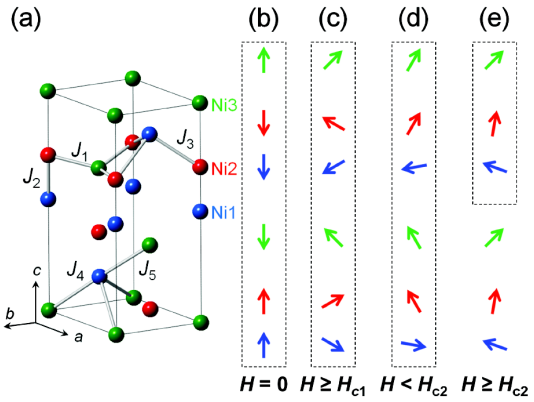

FIG. 1. (a) Crystal structure of Ni_3TeO_6. Only Ni ions are shown.c (b)-(e) Schematic spin structure at different magnetic field values applied along the c-axis. J_i stands for the five nearest-neighbor exchange constants considered in the text. Dotted boxes indicate the magnetic unit cell along the c-axis, which is doubled for (b)-(d) but not (e).

transport method [19]. Magnetization (M) above 13 T was measured in a pulse magnet by recording the induced voltage in a triply-compensated coil [23] and calibrated by vibrating sample magnetometry measurements in a superconducting magnet (PPMS-14, Quantum Design). Magnetostriction ($\Delta L/L$) was measured up to 92 T along the c-axis using an optical fiber grating technique [24]. During the magnetostriction measurement, the ab-plane of the sample was attached to a platform for mechanical stabilization during the rapid magnetic field pulse. The absolute value of magnetostriction was checked and calibrated against a capacitive dilatometer measurement in a superconducting magnet up to 13 T [25]. Hexagonal shaped platelet-like crystals (typically 0.5 mm^2 in area and 90 μm thick) were used for dielectric constant (ε) and P measurements along the c-axis. Electric polarization was obtained under pulsed-field conditions by measuring the magnetoelectric current and integrating it over time [22, 26]. High magnetic fields were generated using either a capacitor-driven pulse magnet up to 65 T or a hybrid pulse magnet (combination of generator- and capacitor-driven magnets) up to 92 T at NHMFL in Los Alamos.

Fig. 2(a) shows the magnetic-field dependence of the magnetization M along the c-axis of NTO up to 92 T. At 4 K a sharp spin-flop transition is evident at $H_{c1} \sim 9$ T, then M increases quasi-linearly up to $\sim$20 T. The linear extrapolation of the $M(H)$ data between 9 and 20 T has a zero intercept at H = 0, consistent with a SF transition. When H is further increased above $\sim$30 T, the slope of the $M(H)$ curve decreases slightly. At H_{c2} = 52 T, a small jump in M is observed, smaller than that at H_{c1}. With further increasing H, M increases linearly up to 92 T. The value of M at 92 T is $\sim$4.8 μ_B per formula unit (f.u.), which is still smaller than the expected saturation magnetization $M_S = 6$ μ_B/f.u. for three Ni^{2+} ions with S = 1 (assuming gyromagnetic ratio of 2). By assuming that there are no other field-induced transi-

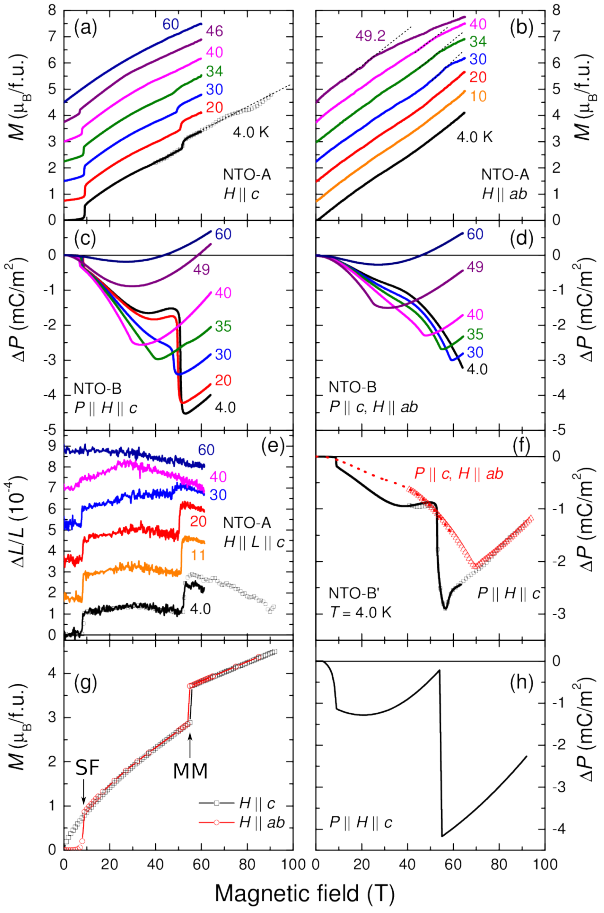

FIG. 2. (a), (b) Magnetization and (c), (d) change of c-axis electric polarization ($\Delta P \equiv P(H) - P(H = 0)$) of Ni_3TeO_6 for magnetic fields applied along various crystalline axes as indicated. (e) c-axis magnetostriction as a function of magnetic field applied along the c-axis. (f) ΔP along c measured up to 92 T for $H \parallel ab$ and $H \parallel c$. (g), (h) The magnetic field dependence of c-axis magnetization $M(H)$ and electric polarization $\Delta P(H)$ in $H \parallel c$ configuration obtained from the model calculations described in text using the exchange constant $J^{\text{PBE0-adj}}$ and exchange-striction parameters listed in Table I. Dashed lines in (a), (b) are guides for the eyes. For clarity, (a), (b) magnetization and (c) magnetostriction curves are shifted by 0.5 μ_B/f.u. and 1.75 $\times$ 10^{-4}, respectively. (e) Jump in magnetostriction at H_{c2} shows a slight difference in magnitude between different types of magnet used, possibly due to the variation in magnetic field sweep rate. Lines and open symbols in (f) denote data taken by using a capacitor-bank-driven pulse magnet and a hybrid pulse magnet, respectively. A single ferroelectric domain sample was used for (c), (d) while a multi-domain (as-grown) sample was used for (f).

tions, linear extrapolation of the high field $M(H)$ curve to the expected M_S value gives a saturation magnetic field H_S of $\sim$ 120 $\pm$ 10 T.

The most striking feature of the high field transition in NTO is the colossal change of P at H_{c2} and reversal of the $\Delta P(H)$ slope at higher fields. Fig. 2(c) shows the change of c-axis electric polarization $\Delta P \equiv P(H) - P(H = 0)$ as a function of magnetic field applied along the c-axis. In this configuration,

the high-field experiment reproduces the step in the $\Delta P(H)$ curve at H_{c1} as previously reported [19]. When the magnetic field is further increased at 4 K, P slightly increases, and then shows a sudden drop at 50 T, close to H_{c2}, with a minimum at 53 T. Counter-intuitively, the change of P at H_{c2} is ~ 10 times larger than that at H_{c1}, whereas the ΔM at H_{c2} is almost two times smaller than that at H_{c1}. When the magnetic field is further increased above 53 T, P increases linearly up to 65 T. We further explored $\Delta P(H)$ up to 92 T, with a different, ferroelectrically multi-domain as-grown sample. In Fig. 2(f), we show that the electric polarization increase linearly above H_{c2}, up to 92 T. A linear extrapolation of $\Delta P(H)$ above H_{c2} gives $\Delta P(H) = 0$ at $H_S = 120 \pm 5$ T, consistent with the linear extrapolation of the $M(H)$ curve. This implies that the magnetically-induced electric polarization is no longer active when the system is in the fully saturated phase. At elevated temperatures, the sharp change of P at H_{c2} still remains, although its magnitude and transition field decreases up to 30 K, above which the sharp drop is replaced with a slope change in the $\Delta P(H)$ curve.

We note that, although NTO shows a strong ME coupling, ΔP displays no dependence on electric poling direction at either magnetic transitions (the details of electric poling dependences are described in the Supplement [27]), suggesting that it is not a type-II multiferroic where magnetic order induces ferroelectricity [5]. Rather, the magnetic order modifies the existing electric polarization associated with the polar space group ($R3$) which is established already at very high temperature (a possible ferroelectric transition temperature of $\sim$ 1000 K was suggested by Ivanov *et al.* [28]).

The lattice also responds sensitively to magnetic field at these transitions in NTO. Fig. 2(e) shows the c-axis magnetostriciton $\Delta L/L$ at different temperatures. Both transitions are accompanied by a large and sudden change of the lattice. At base temperature, $\Delta L/L$ changes sharply ($\sim 40 \times 10^{-6}$) at H_{c1}; above H_{c1}, $\Delta L/L$ initially increases up to $\sim$ 30 T and decreases slightly as magnetic field increases, in accordance with $M(H)$ and $\Delta P(H)$ curves; at H_{c2}, $\Delta L/L$ jumps by $\sim 60 \times 10^{-6}$ and decreases at higher fields.

The in-plane $M(H)$ data (Fig. 2(b)) below 30 K show a monotonic increase under magnetic field. However, above 30 K a clear cusp is observed at the same magnetic field, at which the polarization reversal occurs (Fig. 2(d)). Finally, the electric polarization measured up to 92 T, in an as-grown (multi-domain) sample, shows that the polarization reversal takes place at 70 T at 4 K. Above 70 T, two $\Delta P(H)$ curves measured in different configurations coincide with each other (Fig. 2(f)).

To visualise the giant response of P to the external magnetic field, we plot the ME coefficient $\alpha(\equiv dP/dH)$ of NTO as a function of magnetic field in Fig. 3. In the case of c-axis magnetic field, one can immediately see that the ME coefficient at H_{c2} is almost four times greater than that at H_{c1}, cf. Fig. 3(a). The α value at H_{c2} reaches up to 6×10^3 ps/m which is one of very high α value observed among the magnetoelectric materials to date [29–31].

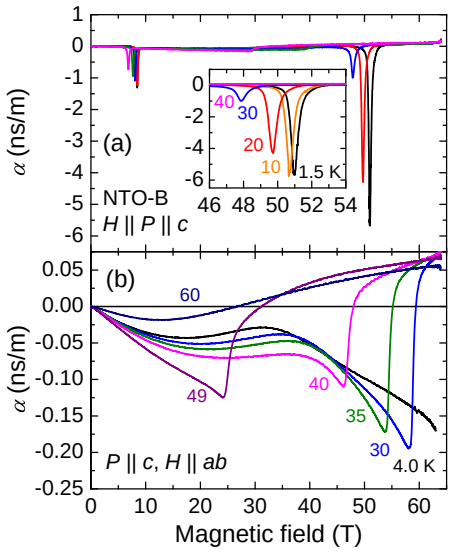

FIG. 3. Magnetoelectric coefficient α as a function of magnetic field for (a) $H \parallel c$ and (b) $H \parallel ab$. Inset in (a) shows a expanded plot of α at the high field transition.

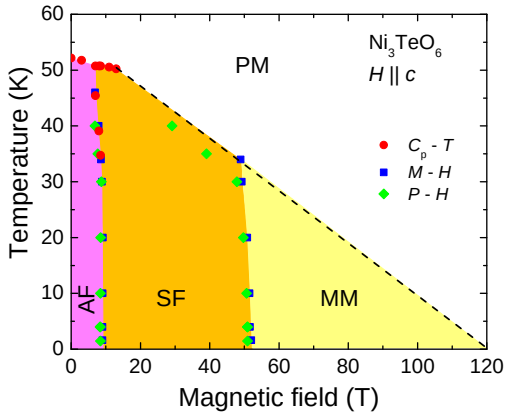

FIG. 4. H-T phase diagram of Ni_3TeO_6 with magnetic field applied along the c-axis determined by peak positions in dM/dH, and $\alpha \equiv$dP/dH, and specific heat (C_p, see Supplement [27]), (Fig. 3) curves. Three distinct phases are identified by measurement up to 92 T at low temperatures. Dashed line is a guide for the eyes.

Using our experimental results, we can construct an H-T phase diagram for NTO in magnetic field along the c-axis, shown in Fig. 4. We observe three ordered phases below T_N: AFM, SF, and metamagnetic phase (MM) which are separated by phase boundaries, almost vertical at low temperatures. The high-temperature phase boundary between the PM and the ordered phase (dotted line in Fig. 4) extrapolates linearly to 120 T at $T = 0$, consistent with the extrapolation of the $M(H)$ and $\Delta P(H)$ curves to their expected saturation and zero values, respectively.

Turning now to the theoretical modeling of this material,

we note that the phenomenological description of magnetism in NTO [19] is applicable in the vicinity of the low-field SF transition, but may not be accurate away from it. In order to study magnetic transitions in the whole magnetic field range, here we use a simplified microscopic model with the Hamiltonian

$$\mathcal{H} = \sum_{i,j} J^{(ij)} \vec{S}_i \cdot \vec{S}_j + \sum_i \left[-K_{2,i} (S_{i,z})^2 - \vec{H} \cdot \vec{S}_i \right], \quad (1)$$

where we model the Ni spins $\vec{S}_i$ (Ni^{2+}, $S = 1$) classically, and i, j run over all Ni sites in the lattice. A previous neutron diffraction study concluded that all three inequivalent Ni sites in the crystallographic unit cell are magnetic [13]. The exchange constants between Ni spins are $J^{(ij)}$, taking particular values $J_1 \ldots J_5$ for the bonds (ij) indicated in Fig. 1. We neglected anisotropic exchanges as well as next-nearest-neighbor Heisenberg exchanges, since the second transition appears in the model without them. The terms with K_2 and $\vec{H}$ model single-ion easy-c-axis anisotropy and the coupling to a uniform magnetic field, respectively.

The exchange constants depend on the ionic coordinates, and as a result, the ions shift in response to spin reorientations in such a way as to strengthen the exchanges that favor the existing spin arrangement. These shifts of charged ions in a polar structure result in a change of electric polarization, which, assuming Heisenberg exchange striction dominates, can be expressed (neglecting higher-order terms containing $(\vec{S}_i \cdot \vec{S}_j)^2$) as

$$\Delta P_c = \sum_n \alpha_n \vec{S}_n \cdot \vec{S}'_n, \quad (2)$$

where P_c is the polarization along c-axis, $\vec{S}_n$ and $\vec{S}'_n$ are the spins connected by the exchange interaction J_n, and the α_n are exchange-striction parameters. We use Eq. (2) to model the dependence of the polarization P on the spin configuration.

The coefficients $\alpha_n = \alpha_{\text{n,ion}} + \alpha_{\text{n,el}}$, with the two terms describing the polarization contributions due to ion shifts and deformations of electronic orbitals, respectively, are calculated using DFT, as described in the Supplement [27].

The determination of exchange constants J_n is a difficult problem. The values calculated previously using DFT [12] give a non-collinear ground state when the energy is minimized within a magnetic unit cell at a realistic values of K_2. We have found that the exchange constants estimated using the PBE0 hybrid functional approximation to DFT [32] give the correct ground state and reproduce the second transition. We have then adjusted these constants to better fit the experimental $M(H)$ data measured along the c-axis. The resulting J_n parameters are summarized in Table I. The exchange-striction constants α_n were calculated using DFT+U, as described in the Supplement [27].

With these model parameters in hand, we computed the changes in the spin arrangement under an applied magnetic field along c; the results are shown in Fig. 1(b-e). The resulting magnetization and polarization curves, presented in Fig. 2(g,h), are in qualitative agreement with experiment. We checked that the calculated transition sequence and spin structures did not change significantly with tuning of the exchange constants, suggesting an absence of competing phases. Our confidence in our correct identification of the phase transitions is further reinforced by the agreement of the calculated and measured magnetization and polarization curves.

In the textbook spin-flop transition for a two-sublattice antiferromagnet, the antiferromagnetic exchange favors the collinear state [33]. Surprisingly, in NTO the situation is the opposite – the antiferromagnetic exchange J_5 actually favors the canted state. Ferromagnetic exchange J_2 favors the collinear state, in which the spins of Ni1 and Ni2 are parallel to each other, as shown in Fig. 2. The evolution of energy contributions from different exchanges under the applied magnetic field is illustrated in the Supplement [27]. In the canted state, above H_{c1}, the spins of Ni1 and Ni2 are no longer parallel thus losing the energy on J_2, but this canting allows a gain in energy from other exchange interactions, while gaining Zeeman energy from the canting of the Ni2 and Ni3 spins along the magnetic field, as shown in Fig. 2(c).

As the magnetic field is increased further above H_{c1}, the spin of the Ni2 rotates. At high fields the c-component of the spins is pinned by the field, while the ab-plane components are chosen to minimize the energy (Eq. 1). This is similar to the energy of the collinear state, except that the ab-component is not constrained to have the unit length. That is why the state that results above H_{c1}, with six spins pointing, right-0-left-right-0-left, differs from the zero-field state, up-up-down-down-down-up. Above H_{c2}, the spin of the Ni1 cants further along the magnetic field, and simultaneously the ab-plane components of the spins in half of the magnetic unit cell reverse in order to gain energy on the antiferromagnetic J_5 exchange, acting between Ni1 and Ni3 spins from the neighboring crystallographic unit cells. At the same time the energy contributions from all the other exchanges increase, as evidenced by the total energy calculation [27]. A reversal of the ab-plane components of the spins in every second crystallographic unit cell leads to a large change of the magnetically-induced electric polarization and strains, as seen in Fig. 2(c,e,h). We can see a restoration of translational symmetry along the c-axis that was broken by antiferromagnetic ordering.

While the magnetic single-ion anisotropy plays an important role for the SF transition, the second transition at H_{c2} is controlled by the magnetic exchanges and the external magnetic field, and is not sensitive to the single-ion anisotropy, thus it is not a classical SF transition. Our model predicts the transition at H_{c2} for both $H \parallel c$ and $H \parallel ab$. Experimentally, however, a sharp transition is not observed in $H \parallel ab$, but there is a cusp in the magnetization curves at around $H \sim 70$ T at $T = 4$ K, suggesting that the transition is of the second order. As is seen in Fig. 3, the magnetization curves and c-axis electric polarization with magnetic field applied different direc-

TABLE I. Exchange, J_n, easy-axis anisotropy constants K_2, and exchange striction parameters for electronic ($\alpha_{n,\text{el}}$) and ionic contributions ($\alpha_{n,\text{ion}}$) to the electric polarization estimated using DFT calculations and adjusted to ensure an antiferromagnetic ground state.

n	1	2	3	4	5	K_2 (meV)
J_n^{GGA}(meV)	-0.6	-3.1	2.2	4.2	1.0	
$J_n^{\text{GGA-adj}}$(meV)	-0.6	-3.1	2.2	4.2	0.69	
$\alpha_{n,\text{el}}$	0.25	3.3	-0.1	-3.0	-0.8	
$\alpha_{n,\text{ion}}$	-2.4	-1.6	-2.0	11.2	6.2	
J_n^{PBE0}(meV)	-1.13	-2.97	0.79	2.76	0.32	0.05
$J_n^{\text{PBE0-adj}}$(meV)	-0.69	-3.63	0.76	3.26	0.65	0.1

tions nearly coincide above the transition, implying that the magnetic states for H along c and ab-plane above the transition are similar. This discrepancy between the theory and experiment could be due to the currently neglected DM interactions and symmetric anisotropic exchanges, which could be important in the strongly noncentrosymmetric, pyroelectric NTO, and could give rise to a spin cycloid state. These possibilities will be the subject of a future investigation.

In summary, a high-field study of NTO reveals the presence of a second spin reorientation transition well above the known spin-flop transition at ~ 9 T. The high-field transition is first-order at 52 T for $H \parallel c$ ($T = 4$ K), and is second-order at 70 T for $H \parallel ab$. Our theoretical analysis suggests that this high-field transition is governed by the competition between the Zeeman and magnetic exchange energies, and entails the reversal of the ab-plane component of half of the spins, leading via the Heisenberg exchange striction to a change of electric polarization that is among the largest observed to date. This spin reorientation results in restoration of translational symmetry along the c-axis that was broken by antiferromagnetic ordering. Our calculations also identify particular exchange interactions that are responsible for the stabilization of the magnetic phases in NTO.

The NHMFL Pulsed Field Facility is supported by the NSF, the U.S. D.O.E., and the State of Florida through NSF cooperative grant DMR-1157490. Work at LANL was supported by the U.S. D.O.E. BES project "Science at 100 tesla" (BES FWP LANLF100). The work at Rutgers was supported by the NSF grants DMREF-1104484, DMREF 12-33349, and the Rutgers IAMDN.

* These authors contributed equally to the present work.

[1] N. A. Spaldin and M. Fiebig, Science **309**, 391 (2005).
[2] W. Eerenstein, N. D. Mathur, and J. F. Scott, Nature **442**, 759 (2006).
[3] S.-W. Cheong and M. Mostovoy, Nat. Mater. **6**, 13 (2007).
[4] T. Kimura, Annu. Rev. Mater. Res. **37**, 387 (2007).
[5] D. I. Khomskii, Physics **2**, 20 (2009).
[6] T. Arima, J. Phys. Soc. Jpn. **80**, 052001 (2011).
[7] H. Katsura, N. Nagaosa, and A. V. Balatsky, Phys. Rev. Lett. **95**, 057205 (2005).
[8] M. Mostovoy, Phys. Rev. Lett. **96**, 067601 (2006).
[9] I. Sergienko and E. Dagotto, Phys. Rev. B **73**, 094434 (2006).
[10] Y. Choi, H. Yi, S. Lee, Q. Huang, V. Kiryukhin, and S.-W. Cheong, Phys. Rev. Lett. **100**, 047601 (2008).
[11] T. Arima, J. Phys. Soc. Jpn. **76**, 073702 (2007).
[12] F. Wu, E. Kan, C. Tian, and M.-H. Whangbo, Inorg. Chem. **49**, 7545 (2010).
[13] I. Živković, K. Prša, O. Zaharko, and H. Berger, J. Phys.: Condens. Matter **22**, 056002 (2010).
[14] M. Hudl, R. Mathieu, S. A. Ivanov, M. Weil, V. Carolus, T. Lottermoser, M. Fiebig, Y. Tokunaga, Y. Taguchi, Y. Tokura, and P. Nordblad, Phys. Rev. B **84**, 180404(R) (2011).
[15] S. A. Ivanov, P. Nordblad, R. Mathieu, R. Tellgren, C. Ritter, N. V. Golubko, E. D. Politova, and M. Weil, Mater. Res. Bull **46**, 1870 (2011).
[16] W. Li, C. Wang, D. Hsu, C. Lee, C. Wu, C. Chou, H. Yang, Y. Zhao, S. C. J. W. Lynn, and H. Berger, Phys. Rev. B **85**, 094431 (2012).
[17] R. Sankar, G. J. Shu, B. K. Moorthy, R. Jayavel, and F. C. Chou, Dalton Trans. **42**, 10439 (2013).
[18] S. A. Ivanov, R. Tellgren, C. Ritter, P. Nordblad, R. Mathieu, G. Andre, N. V. Golubko, E. D. Politova, and M. Weil, Mater. Res. Bull **47**, 63 (2012).
[19] Y. S. Oh, S. Artyukhin, J. J. Yang, V. Zapf, J. W. Kim, D. Vanderbilt, and S.-W. Cheong, Nat. Commun. **5**, 3201 (2014).
[20] M. Herak, H. Berger, M. Prester, M. Miljak, I. Živković, O. Milat, D. Drobac, S. Popović, and O. Zaharko, J. Phys.: Condens. Matter **17**, 7667 (2005).
[21] J. Her, C. Chou, Y. Matsuda, K. Kindo, H. Berger, K. Tseng, C. Wang, W. Li, and H. Yang, Phys. Rev. B **84**, 235123 (2011).
[22] J. W. Kim, Y. Kamiya, E. D. Mun, M. Jaime, N. Harrison, J. D. Thompson, V. Kiryukhin, H. T. Yi, Y. S. Oh, S.-W. Cheong, C. D. Batista, and V. S. Zapf, Phys. Rev. B **89**, 060404(R) (2014).
[23] J. A. Detwiler, G. M. Schmiedeshoff, N. Harrison, A. H. Lacerda, J. C. Cooley, and J. L. Smith, Phys. Rev. B **61**, 402 (2000).
[24] R. Daou, F. Weickert, M. Nicklas, F. Steglich, A. Haase, and M. Doerr, Rev. Sci. Inst. **81**, 033909 (2010).
[25] G. M. Schmiedeshoff, A. W. Lounsbury, D. J. Luna, S. J. Tracy, A. J. Schramm, S. W. Tozer, V. F. Correa, S. T. Hannahs, T. P. Murphy, E. C. Palm, A. H. Lacerda, S. L. Budko, P. C. Canfield, J. L. Smith, J. C. Lashley, and J. C. Cooley, Rev. Sci. Instrum. **77**, 123907 (2006).
[26] V. Zapf, M. Kenzelmann, F. Wolff-Fabris, F. Balakirev, and Y. Chen, Phys. Rev. B **82**, 060402 (2010).
[27] See supplemental material at http://link.aps.org/supplemental/XX.XXXX/PhysRevLett.XXX.XXXXXX for poling electric field-dependence of $\Delta P(H)$, specific heat, and details of DFT calculations.
[28] S. A. Ivanov, R. Mathieu, P. Nordblad, R. Tellgren, C. Ritter, E. Politova, G. Kaleva, A. Mosunov, S. Stefanovich, and M. Weil, Chem. Mater. **25**, 935 (2013).
[29] S. H. Chun, Y. S. Chai, Y. S. Oh, D. Jaiswal-Nagar, S. Y. Haam, I. Kim, B. Lee, D. H. Nam, K.-T. Ko, J. H. Park, and K. H. Kim, Phys. Rev. Lett. **104**, 037204 (2010).
[30] N. Lee, C. Vecchini, Y. J. Choi, L. C. Chapon, A. Bombardi, P. G. Radaelli, and S.-W. Cheong, Phys. Rev. Lett. **110**, 137203 (2013).
[31] T. Toyama, K. Yamauchi, A. Iyama, S. Picozzi, K. Shimizu, and T. Kimura, Nat. Comms. **5**, 4927 (2014).
[32] C. Adamo and V. Barone, J. Chem. Phys. **110**, 6158 (1999).
[33] L. D. Landau, E. M. Lifshitz, and L. P. Pitaevskii, *Electrodynamics of Continuous Media, chapter 50*, 2nd ed., Vol. 8 (Butterworth-Heinemann, 1984).